

4-1-2007

# Warm HCN, C<sub>2</sub>H<sub>2</sub>, and CO in the Disk of GV Tau

E L. Gibb

*University of Missouri*

K.A. VanBrunt

*University of Missouri*

Sean D. Brittain

*Clemson University, sbritt@clemson.edu*

T.W. Rettig

*University of Notre Dame*

Follow this and additional works at: [https://tigerprints.clemson.edu/physastro\\_pubs](https://tigerprints.clemson.edu/physastro_pubs)



Part of the [Astrophysics and Astronomy Commons](#)

---

## Recommended Citation

Please use publisher's recommended citation.

This Article is brought to you for free and open access by the Physics and Astronomy at TigerPrints. It has been accepted for inclusion in Publications by an authorized administrator of TigerPrints. For more information, please contact [kokeefe@clemson.edu](mailto:kokeefe@clemson.edu).

## WARM HCN, C<sub>2</sub>H<sub>2</sub>, AND CO IN THE DISK OF GV TAU

E. L. GIBB AND K. A. VAN BRUNT

Department of Physics and Astronomy, University of Missouri, St. Louis, MO 63121

S. D. BRITAIN

Department of Physics and Astronomy, Clemson University, Clemson, SC 29631

AND

T. W. RETTIG

Department of Physics, University of Notre Dame, Notre Dame, IN 46556

Received 2006 September 27; accepted 2007 February 2

### ABSTRACT

We present the first high-resolution, ground-based observations of HCN and C<sub>2</sub>H<sub>2</sub> toward the T Tauri binary star system GV Tau. We detected strong absorption due to HCN  $\nu_3$  and weak C<sub>2</sub>H<sub>2</sub> [ $\nu_3$  and  $\nu_2 + (\nu_4 + \nu_5)_+^0$ ] absorption toward the primary (GV Tau S) but not the infrared companion. We also report CO column densities and rotational temperatures, and present abundances relative to CO of HCN/CO  $\sim 0.6\%$  and C<sub>2</sub>H/CO  $\sim 1.2\%$  and an upper limit for CH<sub>4</sub>/CO  $< 0.37\%$  toward GV Tau S. Neither HCN nor C<sub>2</sub>H<sub>2</sub> were detected toward the infrared companion, and results suggest that abundances may differ between the two sources.

*Subject headings:* infrared: ISM — ISM: abundances — ISM: molecules — planetary systems: protoplanetary disks

### 1. INTRODUCTION

GV Tau (Haro 6-10, IRAS 04263+2426) is an unusual young T Tauri binary system partly embedded in the L1524 molecular cloud. It is one of a small number of young binaries for which the primary (GV Tau S) is optically visible and the infrared companion (IRC; GV Tau N), located 1.2'' to the north, is strongly extinguished. The spectral energy distribution (SED) of the primary is flat or rising in the 1–100  $\mu\text{m}$  range, suggesting that it is a class I object (Koresko et al. 1999). Leiner & Haas (1989) found that the IRC was generally brighter than the primary at wavelengths longer than  $\sim 4 \mu\text{m}$ . It has also been found that the system is variable, particularly in the near infrared, and on timescales as short as a month (Leinert et al. 2001; Koresko et al. 1999). Leinert et al. (2001) found that the primary became redder as it became fainter in the *K* band. The depth of the 3  $\mu\text{m}$  ice band was also found to vary with time, and their results suggested that an increase in optical depth corresponded to a decrease in *K* brightness. Both of these measurements are consistent with the dominant mechanism of the variability of GV Tau S being due to inhomogeneities in circumstellar material that result in changes in extinction. The behavior for the IRC is more complex and suggests the possibility of variable accretion mechanisms (Leinert et al. 2001).

The system shows a parsec-scale Herbig-Haro flow with a well-defined axis, as well as other smaller flows, one of which is associated with the IRC, and one that does not appear to be associated with either object (Devine et al. 1999). Near-infrared emission images suggest the presence of a flattened circumbinary envelope with a semimajor axis of  $\sim 1000$ – $1500$  AU seen nearly edge-on as the source of the observed polarization and part of the extinction toward both objects (Ménard et al. 1993). We note that their observations do not exclude the additional presence of circumstellar disks around one or both objects.

In this paper we report high-resolution near-infrared detections of CO, HCN, and C<sub>2</sub>H<sub>2</sub> toward GV Tau S. For the IRC, CO was detected in absorption, but HCN and C<sub>2</sub>H<sub>2</sub> were not. In § 2

we discuss the observations and data analysis. In § 3 we present the results of analysis for HCN, C<sub>2</sub>H<sub>2</sub>, and CO, along with upper limits for CH<sub>4</sub>. Results are discussed in § 4.

### 2. OBSERVATIONS AND DATA REDUCTION

High-dispersion, infrared observations of GV Tau were taken with the cryogenic echelle spectrometer NIRSPEC at the 10 m W. M. Keck Observatory on Mauna Kea, Hawaii (McLean et al. 1998). NIRSPEC provides a resolving power of  $\sim 25,000$ , which allows for the clean separation of fundamental and excited states of <sup>12</sup>CO, <sup>13</sup>CO, and C<sup>18</sup>O as well as the  $\nu_3$  band of HCN and two strong bands of C<sub>2</sub>H<sub>2</sub> [ $\nu_3$  and  $\nu_2 + (\nu_4 + \nu_5)_+^0$ ]. Table 1 presents the spectral settings, wavelength coverage, and integration times for the spectral orders analyzed in this paper. The *M*- and *K*-band data covering the fundamental and overtone transitions of CO, respectively, were acquired in 2003 March and August. *KL*-band spectra were obtained on 2006 February 17–18 to search for gas-phase absorptions due to organic species toward GV Tau. The infrared companion of GV Tau was observed simultaneously during the 2006 February 17 and 2003 March observations, enabling us to characterize the spectra toward both objects.

Our reduction and analysis procedures are discussed in DiSanti et al. (2001) and Brittain et al. (2003). We summarize them below. Observations in the *L* and particularly in the *M* band are dominated by a thermal ( $\sim 300$  K) background with sky emission lines superposed. In order to cancel atmospheric and background effects, we nodded the telescope between positions one-quarter of the way from the top and bottom of the slit, our “A” and “B” positions, respectively. Each exposure corresponded to 1 minute of integration time. Telluric lines were canceled to first order by combining observations as  $(A-B-B+A)/2$ . A series of flats and darks was taken for each grating setting. After flat-fielding and dark subtraction, systematically hot and dead pixels and cosmic-ray hits were removed, and the data were resampled to align the spectral and spatial dimensions along rows and columns, respectively. Examples of extracted spectra are shown in Figures 1 and 2. The individual lines of each molecule are labeled.

TABLE 1  
OBSERVING LOG

Date	Instrument Setting	Wavelength Coverage (cm <sup>-1</sup> )	Integration Time (s)
2003 Mar 18 .....	MW1	2118–2153 (order 16)	240
2003 Mar 18 .....	MW2	2094–2127 (order 16)	240
2003 Aug 05 .....	K1 <sup>a</sup>	4202–4267 (order 32) 4333–4397 (order 33)	1200
2003 Aug 05 .....	K2 <sup>a</sup>	4265–4326 (order 33)	1200
2006 Feb 17 .....	KL1	3024–3072 (order 23) 3286–3337 (order 25)	240
2006 Feb 18 .....	KL2 <sup>a</sup>	2985–3028 (order 23) 3243–3290 (order 25)	240

<sup>a</sup> The IRC was not in the slit in this observation.

The atmospheric transmittance function was modeled using the Spectrum Synthesis Program (SSP; Kunde & Maguire 1974), which accesses the updated HITRAN 2000 molecular database (Rothman et al. 2003). For each grating setting, the column burdens of atmospheric species, the spectral resolving power, and the wavelength calibrations were established by fitting the optimized model. To extract our spectral absorption features, we subtracted the model, convolved to the resolution of the instrument, from the spectral extract. This results in a residual that is still convolved to the telluric spectrum. For intrinsically narrow lines, we obtain the true line intensity incident at the top of the terrestrial atmosphere by dividing each spectral line by the transmittance at the Doppler-shifted position using the fully resolved model. The optimized model is shown as the dashed line in Figures 1 and 2 and has been found to reproduce the telluric spectrum accurately.

We note that the relative continuum brightnesses of the primary and companion varied significantly between our 2003 and 2006 observations. In particular, the IRC was fainter than GV Tau S through the 2–5  $\mu\text{m}$  region. Both objects are known to vary in the infrared (Leinert et al. 2001), and the variations are thought to be due primarily to variable amounts of intervening gas and dust, essentially clumpy circumbinary material. Leinert et al. (2001) reported that GV Tau S got slightly fainter in the  $M$  band over the period from 1993–2000, while the IRC was found

to get brighter during the same time interval. A similar trend was seen for both objects in the  $L'$  band. In SpeX data acquired in 2004 November, the infrared companion was substantially fainter than GV Tau S throughout the 2–5  $\mu\text{m}$  region. This was also true for our 3.3  $\mu\text{m}$  observations in 2006. Nonetheless, we were able to extract spectra from both GV Tau S and its IRC.

The extinction toward GV Tau S is relatively small ( $A_V \sim 5.6$  mag), and thus we may also be detecting stellar photospheric absorption lines. To check for possible photospheric lines, we compared our spectral type K3 GV Tau spectra (Goodrich 1986) to a high-resolution K2 spectrum of Arcturus (Hinkle et al. 1995). The Arcturus spectrum was Doppler shifted to the geocentric velocity of GV Tau as determined by our HCN and CO observations, which were found to be consistent with the heliocentric velocity measured by White & Hillenbrand (2004), and convolved to the resolution of our NIRSPEC data. Broad (consistent with the rotational broadening reported by White & Hillenbrand [2004]) absorption lines corresponding to photospheric OH and NH were present toward GV Tau S (Fig. 2, *crosses and asterisks*). Contaminated lines were eliminated from our analysis. The remaining absorption features were measured by fitting a Gaussian profile to calculate the equivalent width.

### 3. MOLECULAR ABSORPTIONS TOWARD GV TAU

#### 3.1. CO Gas Spectra

##### 3.1.1. GV Tau S

For GV Tau S, the fundamental ro-vibrational lines of <sup>12</sup>CO, <sup>13</sup>CO, and C<sup>18</sup>O near 4.67  $\mu\text{m}$  and the overtone bands near 2.3  $\mu\text{m}$  were observed in absorption in 2003 March and August, respectively (Fig. 1). Absorption-line studies have the advantage of measuring physical conditions in a pencil-beam column of gas along the line of sight to the emitting source, usually the star and inner accretion disk. This allows us to sample a long path length through the edge-on circumbinary envelope and circumstellar disk. The rotational temperatures and column densities of the different bands and isotopes of CO were derived using a population analysis and are presented in Figure 3 and Table 2. The overall rotational temperature found for CO toward GV Tau S is  $\sim 200$  K, somewhat warmer than that found for HCN (§ 3.2), although within  $3\sigma$  for the overtone lines and lines of C<sup>18</sup>O and

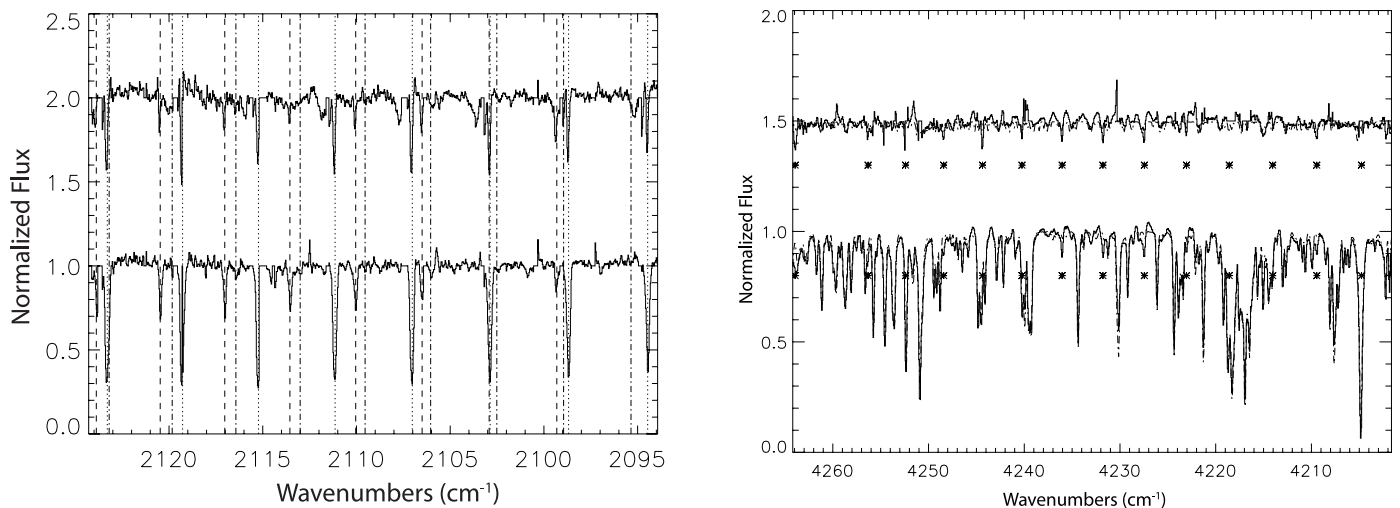


FIG. 1.— (a) Sample-normalized residual  $M$ -band spectrum showing CO absorption toward GV Tau S (bottom) and the IRC (top). The dotted lines indicate positions of the <sup>12</sup>CO lines, the dashed lines indicate <sup>13</sup>CO, and the dot-dashed lines indicate C<sup>18</sup>O. (b) Normalized  $K$ -band spectrum of GV Tau S with the telluric model overplotted (dot-dashed line). Above is the residual with the Arcturus spectrum overplotted, convolved to the resolving power of NIRSPEC, veiled and Doppler shifted to the geocentric velocity of GV Tau. Asterisks indicate the positions of CO(2–0) absorption lines.

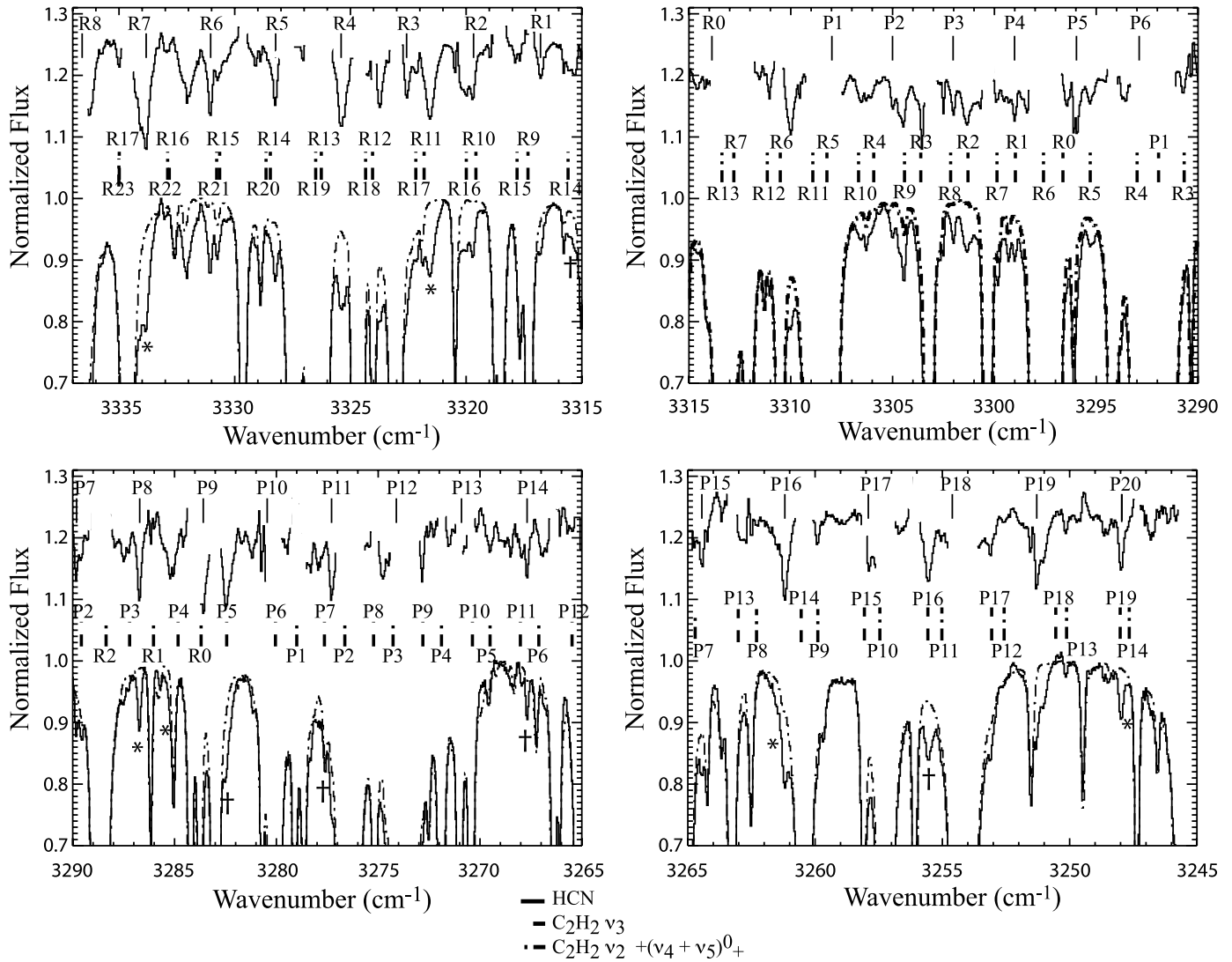


FIG. 2.—GV Tau S, KL Order 25 spectrum showing the positions of HCN and  $C_2H_2$  lines. Solid black ticks are the HCN  $\nu_3$  band, dashed ticks indicate the  $C_2H_2$   $\nu_3$  band, and dot-dashed ticks indicate the  $C_2H_2$  [ $\nu_2 + (\nu_4 + \nu_5)_+^0$ ] band. Asterisks and crosses denote Doppler-shifted positions of stellar OH and NH, respectively.

consistent with the  $T_{\text{rot}}$  found for  $C_2H_2$  (§ 3.4). This is also similar to the warm ( $\sim 100$  K) temperatures we find toward other flared disk systems (Rettig et al. 2006) and implies that the gas is located in the inner, potentially planet-forming ( $\sim 10$  AU or so) region of the circumstellar disk rather than in the more distant interstellar or circumbinary material. The column density of  $^{12}CO$  was found to be  $(5.9 \pm 1.2) \times 10^{18} \text{ cm}^{-2}$  based on an analysis of the overtone lines, which are optically thin. The fundamental lines of CO are optically thick and require a curve-of-growth analysis.

We found  $^{12}CO/^{13}CO$  to be  $54 \pm 15$ , consistent with that measured toward Orion A ( $67 \pm 3$ ; Langer & Penzias 1990) and that found toward the young star HL Tau ( $76 \pm 9$ ; Brittain et al. 2005). The  $^{12}CO/C^{18}O$  ratio is  $420 \pm 170$ , somewhat lower than toward Orion ( $\sim 660$ ; Langer & Penzias 1990), HL Tau ( $800 \pm 200$ ; Brittain et al. 2005), and the canonical interstellar value of  $560 \pm 25$  found by Wilson & Rood (1994). We would expect the isotopic abundance ratios to reflect the isotopic composition of the dense cloud unless influenced by a mechanism such as selective dissociation (Lyons & Young 2005), which may occur since the isotopomers are not self-shielded as effectively as  $^{12}CO$ . This effect does not seem to be evident toward GV Tau.

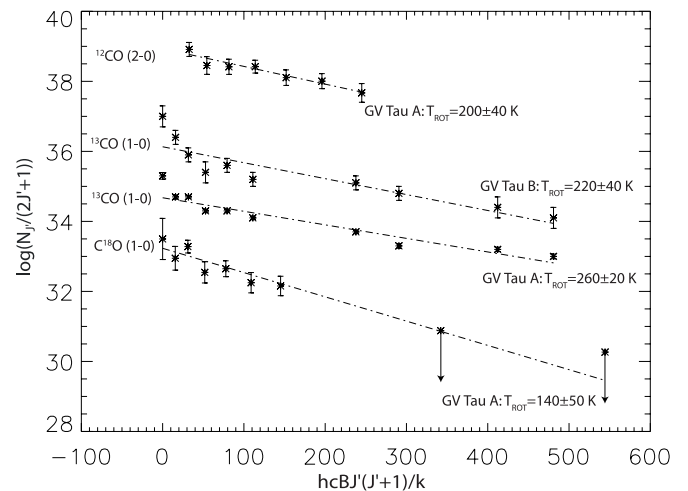


FIG. 3.—Population diagram of the  $^{12}CO(2-0)$ ,  $^{13}CO(1-0)$ , and  $C^{18}O(1-0)$  lines.

TABLE 2

COLUMN DENSITIES AND ROTATIONAL TEMPERATURES FOR MOLECULES

Molecule	Column Density (10 <sup>16</sup> cm <sup>-2</sup> )	$T_{\text{rot}}$ (K)	Abundance Relative to <sup>12</sup> CO (%)
GV Tau S			
<sup>12</sup> CO.....	590 ± 120	200 ± 40	...
<sup>13</sup> CO.....	11	260 ± 20	1.9
C <sup>18</sup> O.....	1.4 ± 0.5	140 ± 50	0.24
HCN.....	3.7 ± 0.3	115 <sup>+11</sup> <sub>-10</sub>	0.63
C <sub>2</sub> H <sub>2</sub> .....	7.3 <sup>+0.1</sup> <sub>-0.2</sub>	170 <sup>+19</sup> <sub>-16</sub>	1.2
CH <sub>4</sub> .....	<2.2	...	<0.37
Infrared Companion			
<sup>12</sup> CO.....	~300 <sup>a</sup>	...	...
<sup>13</sup> CO.....	5.5	220 ± 40	54 <sup>a</sup>
HCN.....	<0.48	...	<0.16

<sup>a</sup> Assuming <sup>12</sup>CO/<sup>13</sup>CO ratio is the same as for GV Tau S.

### 3.1.2. IRC

The infrared companion was observed in the *M* band in 2003 March, but was not placed in the slit during the *K*-band observations. The IRC was resolved and <sup>13</sup>CO was detected, although C<sup>18</sup>O was not. We estimate that the <sup>12</sup>CO column density is  $\sim 3 \times 10^{18}$  cm<sup>-2</sup>, assuming that the <sup>12</sup>CO/<sup>13</sup>CO ratio toward the two objects is the same. This assumption seems reasonable, given that the <sup>12</sup>CO lines toward the IRC are about half as strong as those toward GV Tau S, and in order to bring  $N(^{12}\text{CO})$  for the IRC in agreement with the primary, the <sup>12</sup>CO/<sup>13</sup>CO ratio would have to be a factor of 2 higher. Future observations of the overtone CO lines toward the IRC are planned to directly measure <sup>12</sup>CO.

## 3.2. HCN Gas

### 3.2.1. GV Tau S

Rather strong absorption lines due to the HCN (100–000) band near 3.0 μm were detected toward GV Tau S. Spectral extracts are shown in Figure 2. The geocentric Doppler-shifted positions (+49 km s<sup>-1</sup>) of the HCN absorption lines and the specific identifications are indicated by solid ticks. We performed a rotational analysis on absorption features that were at transmittance >80%, were not blended with C<sub>2</sub>H<sub>2</sub> transitions (also indicated in Fig. 2), and were clear of contamination from stellar absorption features as determined from a comparison to the similar spectral type high-resolution Arcturus spectrum of Hinkle et al. (1995). There were a total of 10 lines that satisfied these criteria, ranging from  $J = 0$  to 7.

Einstein *A*-coefficients and line positions were taken from the ab initio line list calculated by Harris et al. (2002), which expanded on previous line lists and improved accuracy by using the most accurate potential energy surface and dipole moment surface information available. The population diagram is shown in Fig. 4. The Doppler-shifted positions and equivalent widths used are given in Table 3.

We note that the lines in our analysis are optically thin for most reasonable values of the intrinsic line widths ( $b$ ). For example, the R6 line is optically thin ( $\tau < 1$ ) for all  $b > 1.7$  km s<sup>-1</sup>. For R1,  $\tau > 1$  is achieved only for  $b < 0.9$  km s<sup>-1</sup>. Brittain et al. (2005) found  $b = 1.3 \pm 0.1$  for CO toward HL Tau. Lahuis et al. (2006) find that no good fit can be made to the C<sub>2</sub>H<sub>2</sub> and CO profiles for  $b < 2$  km s<sup>-1</sup>. Boogert et al. (2002) find that  $0.8 < b < 1.5$  km s<sup>-1</sup> toward L1489 to explain the CO observations.

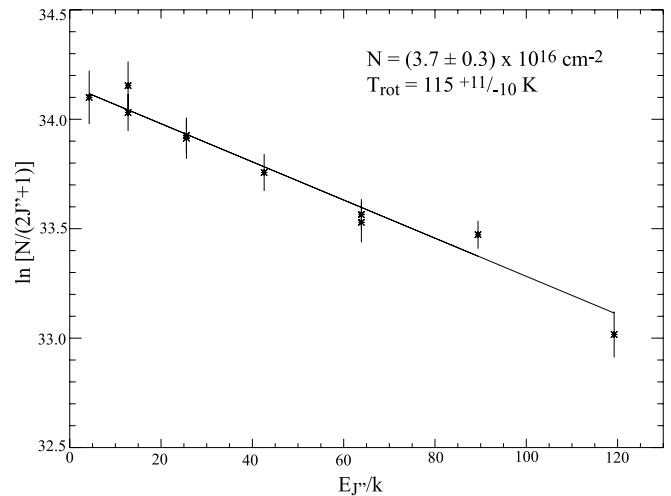


FIG. 4.—Population diagram for HCN absorption toward GV Tau S.

If we make a reasonable assumption that  $b > 1$  km s<sup>-1</sup>, then our absorptions are optically thin. This is also supported by the linearity of the population diagram. From this, we derive a rotational temperature of  $115^{+11}_{-10}$  K and a total HCN column density of  $(3.7 \pm 0.3) \times 10^{16}$  cm<sup>-2</sup> toward GV Tau S. Comparing this to the CO column density (§ 3.1) provides an HCN/CO  $\sim 0.63\%$ .

### 3.2.2. IRC

Interestingly, HCN absorption was not seen toward the infrared companion star. If we assume the same  $T_{\text{rot}}$  as found for the primary (115 K), the  $3\sigma$  upper limit for the HCN column density toward the infrared companion is  $4.8 \times 10^{15}$  cm<sup>-2</sup>, a factor of about 8 lower than the primary. The estimated CO column density toward the IRC is a factor of 2 less than toward GV Tau S. If we assume that the CO absorption originates in the inner circumstellar disk of each object, then the resulting difference in HCN column densities implies that HCN is at least a factor of 4 less abundant toward the IRC. This result is important. The fact that the HCN column density is significantly lower toward the IRC is a strong constraint that argues for the HCN being located in the warm inner disk of the primary, rather than in the interstellar medium or the circumbinary material that surrounds both objects.

This result may suggest that there are significant compositional differences between the inner disk ( $\sim 10$  AU or so) material toward the two objects. However, we point out that caution must be used when comparing the primary to the IRC. There is no a priori reason to assume the same gas temperature toward both objects if the gas is associated with a circumstellar disk rather than the circumbinary material. The IRC was not located in the slit during our KL2 observation (Table 1). This means that only the  $J < 8$  transitions of HCN were covered. Because of the fact that only low- $J$  lines were sampled toward the IRC, the upper limit is less constrained for higher temperatures. For example, if we assume  $T = 400$  K, then the upper limit for  $N(\text{HCN})$  becomes  $\sim 1.1 \times 10^{17}$  cm<sup>-2</sup>.

## 3.3. CH<sub>4</sub> Gas

We attempted to detect CH<sub>4</sub> in our *KL*-band, order 25 setting, which covered several transitions. With a geocentric Doppler shift of +49 km s<sup>-1</sup> during the observations, the lines should have been shifted out of the telluric features to transmittances ranging from  $\sim 60\%$  for P2, up to  $\sim 80\%$  for R0 and P1, to  $86\%$

TABLE 3  
HCN LINE POSITIONS AND EQUIVALENT WIDTHS

Line ID	$\nu_{\text{rest}}$ ( $\text{cm}^{-1}$ )	$\nu_{\text{shift}}$ ( $\text{cm}^{-1}$ )	$v_{\text{rad}}$ ( $\text{km s}^{-1}$ )	Percent Transmittance ( $\text{cm}^{-1}$ )	$W \pm dW$
P7 .....	3290.35	3289.81	49	0.91	$0.0154 \pm 0.0016$
P5 .....	3296.49	3295.92	52	0.91	$0.0184 \pm 0.0016$
P4 .....	3299.53	3299.01	48	0.95	$0.0183 \pm 0.0016$
P3 .....	3302.53	3302.02	48	0.97	$0.0162 \pm 0.0015$
P2 .....	3305.54	3304.97	52	0.98	$0.0136 \pm 0.0015$
R1 .....	3317.33	3316.77	50	0.95	$0.0128 \pm 0.0016$
R2 .....	3320.22	3319.69	48	0.98	$0.0179 \pm 0.0015$
R3 .....	3323.09	3322.54	50	0.89	$0.0212 \pm 0.0016$
R5 .....	3328.78	3328.25	47	0.95	$0.0222 \pm 0.0016$
R6 .....	3331.59	3331.07	47	0.98	$0.0236 \pm 0.0015$

for R1. From this, we calculated a  $3\sigma$  upper limit for the  $\text{CH}_4$  column density of  $<2.2 \times 10^{16} \text{ cm}^{-2}$  using the methodology discussed in Gibb et al. (2004) and assuming the same rotational temperature as that found for HCN (115 K). When compared with the HCN and CO, we find that  $\text{CH}_4/\text{HCN} < 60\%$  and  $\text{CH}_4/\text{CO} < 0.37\%$ . This is not as well constrained as the gas-phase  $\text{CH}_4/\text{CO}$  ratio found for HL Tau (Gibb et al. 2004), but it is still substantially smaller than the overall  $\text{CH}_4/\text{CO}$  ratio found for comets (Gibb et al. 2003) and somewhat lower than reported for  $\text{CH}_4/\text{CO}$  (ice + gas) for massive YSOs by Boogert et al. (1997, 1998).

### 3.4. $\text{C}_2\text{H}_2$ Gas

There are two comparably strong bands of acetylene in the  $3 \mu\text{m}$  region: the  $\nu_3$  band centered at  $3294.84 \text{ cm}^{-1}$  and the  $\nu_2 + (\nu_4 + \nu_5)_+$  band centered at  $3281.90 \text{ cm}^{-1}$  (see Jacquemart et al. 2003 and references therein). Ordinarily, the  $\nu_3$  band would be 1100 times stronger than the combination mode. However, a Fermi resonance between the two bands causes the combination band to become slightly stronger than the  $\nu_3$  band (Vander Auwera et al. 1993).

From the analysis of the  $3 \mu\text{m}$  spectra (Fig. 2), a number of unblended lines of  $\text{C}_2\text{H}_2$  are detected at relatively good transmittance ( $>80\%$ ). The positions of individual  $\text{C}_2\text{H}_2$  lines are indicated in Figure 3 (dot-dashed ticks). We analyzed 15 unblended lines with high transmittance from the  $\nu_2 + (\nu_4 + \nu_5)_+$  band and four lines of the  $\nu_3$  band to determine the column density (Fig. 5,

Table 4). We also checked for possible contamination due to stellar photospheric features by comparison with an Arcturus spectrum. The rotational temperature analysis yielded a  $T_{\text{rot}} = 170_{-16}^{+19} \text{ K}$ , which is consistent with those found for HCN and CO within the uncertainty, and a total column density of  $(7.3_{-0.2}^{+0.1}) \times 10^{16} \text{ cm}^{-2}$ . These values are consistent with the nondetection of the  $\nu_3$  P18 line, which is at 97% transmittance and unblended. The predicted equivalent width of P18, based on the fit in Figure 5, is  $0.0011 \text{ cm}^{-1}$ , within the  $1\sigma$  noise limit of  $0.0014 \text{ cm}^{-1}$ .

## 4. DISCUSSION

We investigated the composition of several organic molecules toward the binary T Tauri system GV Tau. Such species as HCN,  $\text{C}_2\text{H}_2$ , and  $\text{CH}_4$  are key to understanding the chemical compositions and evolution of the volatile material that becomes incorporated into the planet-forming regions of disks around young stars. We detected HCN and  $\text{C}_2\text{H}_2$  toward the primary and provide upper limits for the IRC. This is only the second reported detection of these species in the gas phase toward a low-mass T Tauri star. The first reported detection of these molecules was via *Spitzer* Infrared Spectrograph (IRS) observations toward IRS 46 in the  $\rho$  Ophiuchus cloud (Lahuis et al. 2006). The warm temperatures ( $\sim 400 \text{ K}$  for HCN and  $\sim 800 \text{ K}$  for  $\text{C}_2\text{H}_2$ ) suggested a possible disk origin for the absorptions, but were not definitive, as Lahuis et al. (2006) could not distinguish whether the gas was located in the disk or a jet.

### 4.1. Location of the Gas toward GV Tau

In 2006 February, HCN was detected toward the primary (GV Tau S; Fig. 2). However, for the IRC, which was observed simultaneously, the lack of a detection suggests a significant lower total column density if we assume the same rotational temperature. Similarly, the CO spectra toward GV Tau S and the IRC are significantly different, suggesting a factor of 2 difference in column density, resulting in a factor of at least 4 lower abundance toward the IRC. This result is a strong indication that the HCN is located close to GV Tau S, within the circumstellar flared disk, and not associated with the IRC (and therefore not in the circumbinary material). The warm rotational temperatures of  $\sim 100\text{--}200 \text{ K}$  determined for HCN,  $\text{C}_2\text{H}_2$ , and CO also suggest a location in the inner region of the disk that surrounds GV Tau S rather than in the circumbinary envelope. A jet origin can likely be eliminated as the Doppler shifts of stellar photospheric absorption lines agree with those found for the intervening molecular material to within  $\sim 5 \text{ km s}^{-1}$ . We derive a heliocentric radial velocity of  $21 \pm 5 \text{ km s}^{-1}$  for CO and  $19.5 \pm 3.4$  for HCN. This is similar to the heliocentric Doppler shift of  $13.4 \pm 3.8 \text{ km s}^{-1}$  reported by White & Hillenbrand (2004) using high-resolution

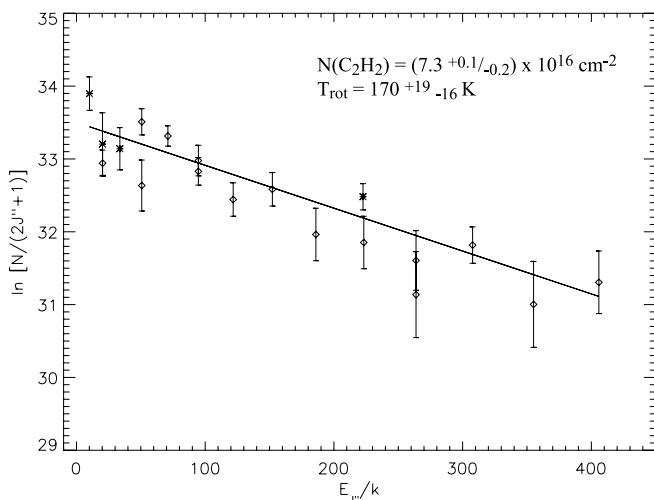


FIG. 5.—Population diagram for  $\text{C}_2\text{H}_2$  absorption toward GV Tau S. Asterisks are data points from the  $\nu_3$  branch, diamonds are from the  $\nu_2 + (\nu_4 + \nu_5)_+$  branch.

TABLE 4  
C<sub>2</sub>H<sub>2</sub> LINE POSITIONS AND EQUIVALENT WIDTHS

Line ID	$\nu_{\text{rest}}$ (cm <sup>-1</sup> )	$\nu_{\text{shift}}$ (cm <sup>-1</sup> )	Percent Transmittance (cm <sup>-1</sup> )	$W \pm dW$
$\nu_3$ Band				
R4.....	3306.48	3305.94	0.96	0.0067 $\pm$ 0.0020
P2.....	3290.13	3289.59	0.86	0.0058 $\pm$ 0.0014
P3.....	3287.75	3287.22	0.96	0.0044 $\pm$ 0.0019
P11.....	3268.48	3267.94	0.97	0.0077 $\pm$ 0.0014
$\nu_2 + (\nu_4 + \nu_5)_+$ Band				
R15.....	3318.35	3317.81	0.90	0.0037 $\pm$ 0.0016
R12.....	3311.71	3311.17	0.88	0.0041 $\pm$ 0.0017
R10.....	3307.22	3306.68	0.95	0.0049 $\pm$ 0.0018
R7.....	3300.42	3299.88	0.91	0.0084 $\pm$ 0.0016
R5.....	3295.84	3295.31	0.95	0.0124 $\pm$ 0.0014
R3.....	3291.23	3290.69	0.86	0.0047 $\pm$ 0.0016
P5.....	3270.05	3269.52	0.94	0.0044 $\pm$ 0.0016
P6.....	3267.66	3267.12	0.94	0.0105 $\pm$ 0.0015
P7.....	3265.26	3264.72	0.78	0.0088 $\pm$ 0.0018
P8.....	3262.84	3262.31	0.95	0.0059 $\pm$ 0.0014
P9.....	3260.43	3259.89	0.84	0.0077 $\pm$ 0.0017
P11.....	3255.56	3255.03	0.84	0.0046 $\pm$ 0.0017
P12.....	3253.12	3252.59	0.95	0.0025 $\pm$ 0.0014
P13.....	3250.66	3250.13	0.98	0.0053 $\pm$ 0.0013
P14.....	3248.20	3247.67	0.95	0.0026 $\pm$ 0.0015
P18.....	3251.09	3250.56	0.97	<0.0014

optical spectra of stellar emission lines. The combination of velocity information, significantly different compositions toward closely spaced objects, and warm rotational temperatures combine to argue that the HCN, C<sub>2</sub>H<sub>2</sub>, and CO are located in the disk of GV Tau S.

If we assume that the near-infrared variability toward GV Tau is due primarily to cooler material in the outer disk or circum-binary envelope rather than the warm material where the CO, HCN, and C<sub>2</sub>H<sub>2</sub> absorptions originate, as suggested by the 3  $\mu\text{m}$  ice feature variability, then we can compare our column densities of HCN and C<sub>2</sub>H<sub>2</sub> to CO (see Table 2). We must be cautious with such an interpretation, however, since our CO (2 and 5  $\mu\text{m}$ ) observations and our 3  $\mu\text{m}$  observations were taken at different times and the sources are both highly variable in the infrared over short timescales. This could affect the amount of gaseous material in the line of sight. For example, tidal interactions between the two stars, which are only separated by about 170 AU, may affect the gas structure close to the stars. Perhaps the temperature and density structures of the inner disks differ, resulting in dissimilar chemical evolution. It may also be possible that an inner circumstellar disk of the IRC is more inclined than the nearly edge-on GV Tau S and that we are seeing warm CO in the flared disk. The molecules in disk atmospheres are less protected from energetic photons than those in the midplane, leading to higher photodissociation rates. Collisional dissociation in the inner disk may act to remove hydrogen atoms from molecules like C<sub>2</sub>H<sub>2</sub> and HCN. In addition, the increased production of ions in disk atmospheres and the resulting ion-molecule chemistry will further modify the composition. The extent to which these processes occur is dependent on the local ionizing radiation field, temperature, and density (see papers by Willacy et al. [1998], Markwick et al. [2002], and Aikawa et al. [1999, 2002] for discussions of chemistry in protoplanetary disks). Hence, the chemistry is dependent on radial and vertical distances in the disk, and

our measurements are correspondingly dependent on viewing geometry. Additional observations to simultaneously measure CO and HCN toward GV Tau are planned to address this issue and to investigate the possibility of variations in column densities of gaseous species.

#### 4.2. Compositional Comparisons

It is interesting to compare our results for GV Tau S to those found toward other young stars, models of chemistry in protoplanetary disks, and comets in our own solar system. Assuming that CO, HCN, and C<sub>2</sub>H<sub>2</sub> originate in the same region, we found a C<sub>2</sub>H<sub>2</sub>/HCN ratio of  $\sim 2.0$  toward GV Tau S and HCN/CO  $\sim 0.63\%$  and C<sub>2</sub>H<sub>2</sub>/CO  $\sim 1.2\%$ . C<sub>2</sub>H<sub>2</sub>/HCN was found to be  $\sim 0.6$  toward IRS 46 (Lahuis et al. 2006), another low-mass object, assuming that both species originate in the same region. The 13–14  $\mu\text{m}$  Q-branches and band heads of C<sub>2</sub>H<sub>2</sub> and HCN were studied by the *Infrared Space Observatory* (ISO; Lahuis & van Dishoeck 2000) toward massive YSOs. In general, C<sub>2</sub>H<sub>2</sub>/HCN for the warm component was found to be  $\sim 40\%$ – $50\%$  toward most objects. Interestingly, HCN was found to be more abundant ( $\sim 2.5\%$ ) toward IRS 46 compared to CO (this is a lower limit). This can be seen graphically in Figure 6. In that figure, C<sub>2</sub>H<sub>2</sub>/HCN is indicated by asterisks while the abundances of C<sub>2</sub>H<sub>2</sub> and HCN relative to CO (in percentages) are indicated by squares and diamonds, respectively.

Markwick et al. (2002) modeled molecular distributions of abundant species in the inner 10 AU of protostellar disks surrounding T Tauri stars. Gibb et al. (2004) measured an upper limit for CH<sub>4</sub>/CO toward HL Tau that was significantly lower than predicted by the model. The same was found for GV Tau S, where CH<sub>4</sub>/CO  $< 0.0037$  is much smaller than the CH<sub>4</sub>/CO  $\sim 1$  predicted by Markwick through most of the inner disk. However, we find that HCN/CO, C<sub>2</sub>H<sub>2</sub>/CO, and C<sub>2</sub>H<sub>2</sub>/HCN ratios toward GV Tau S are in general agreement with the range of abundances

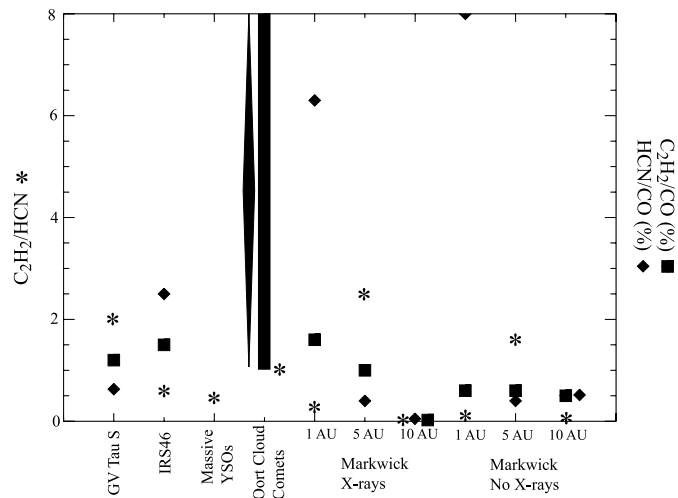


FIG. 6.—Abundances toward GV Tau S, IRS 46, Massive YSOs, Oort Cloud Comets, and the chemical model of Markwick et al. (2002). Asterisks indicate the  $C_2H_2/HCN$  ratio. Squares and diamonds indicate the abundances relative to CO of  $C_2H_2$  and HCN, respectively.

found in Markwick et al. (2002) (see also our Fig. 6). Our rotational temperatures ( $\sim 100$ – $200$  K) are also consistent with the midplane temperatures in the inner  $\sim 5$  AU of the protoplanetary disk in the Markwick model. We note, however, that we are likely sampling a region above the midplane, possibly in a disk atmosphere, which may be heated by various mechanisms such as viscous accretion, X-rays, or an X-wind (see Glassgold et al. [2004] for a discussion of disk heating). This would move the location of the gas outward by an amount depending on the local environment. Nonetheless, the similarity in abundances between Markwick et al. (2002), GV Tau, and IRS 46 is interesting and should be pursued further.

Another interesting comparison is with comets in our own solar system. Comets are generally considered to be the most pristine objects in the solar system and are thought to have formed in the giant-planet region (from  $\sim 5$ – $30$  AU). Infrared spectroscopy has routinely measured abundances of CO, HCN, and  $C_2H_2$  toward comets for the last decade (see Mumma et al. 2003 and references therein). HCN and  $C_2H_2$  abundances measured in comets (compared to water) are fairly consistent over the Oort cloud population measured to date, and the  $C_2H_2/HCN$  ratio is found to be typically  $\sim 0.9$ – $1.1$ , reasonably consistent with the  $C_2H_2/HCN$  ratios of 0.6 and 2.0 found for IRS 46 and GV Tau, respectively. The CO abundance in comets has been found to be highly variable, likely as a result of thermal history and processing of comets in the protoplanetary disk. The resulting HCN/CO and  $C_2H_2/CO$  ratios range from  $\sim 0.01$ – $0.16$ . The HCN/CO and  $C_2H_2/CO$  ratios found in GV Tau and IRS 46 are consistent with those found for CO-rich comets. It is possible that the more volatile CO was preferentially lost in comets for which the HCN/CO or  $C_2H_2/CO$  ratios are high. If we assume that the comets with the greatest abundance of CO more closely represent the initial volatile abundance of the giant-planet-forming region of the solar

nebula, the resulting  $C_2H_2/HCN$ ,  $C_2H_2/CO$ , and HCN/CO ratios agree to within a factor of 2 with those found for GV Tau S, IRS 46, massive YSOs, and several of the Markwick model results.

Also of interest is  $CH_4$ , another particularly volatile molecule for which the abundance (relative to water) has been observed to be highly variable in comets (by over an order of magnitude). While the magnitude of the abundance variation is similar to that found for CO in comets, the two molecules are not correlated (Gibb et al. 2003). In comets  $CH_4/CO$  is found to vary from  $\sim 0.05$ – $0.8$ , much higher than in HL Tau ( $< 0.0002$  in the gas phase) or GV Tau S ( $< 0.0037$ ), and lower than the  $CH_4/CO \sim 1$  found by Markwick et al. (2002).  $CH_4/HCN$  is found to vary from  $\sim 2$ – $5$  among comets yet is  $< 0.6$  toward GV Tau S. The reasons for these compositional differences are unknown, and more work must be done to characterize volatiles toward comets and low-mass star-forming regions.

## 5. CONCLUSION

We have measured column densities and rotational temperatures for CO, HCN, and  $C_2H_2$  and an upper limit for  $CH_4$  toward GV Tau S. We find that the absorptions are consistent with an origin in the inner region of a protoplanetary disk. This conclusion is further strengthened by the lack of absorptions due to organic species toward the infrared companion (IRC) to GV Tau S, although gas-phase CO is present. The upper limit for HCN toward the IRC may suggest compositional differences between the two objects, although a different temperature or viewing geometry cannot be ruled out. We note that GV Tau is variable in the near-infrared, likely due to inhomogeneities in the circum-binary material or outer disk. Future observations in the  $M$  and  $L$  bands are planned to test whether the variability affects the column densities and abundances of the gas-phase species reported in this paper.

We find that the abundances of HCN and  $C_2H_2$  relative to each other and to CO are similar to those found among the comet population, that found toward low-mass object IRS 46 by Lahuis et al. (2006), and consistent with the disk model by Markwick et al. (2002).  $CH_4$ , on the other hand, appears to be underabundant in the young stars sampled to date when compared to comets in our own solar system. This exciting result illustrates the feasibility of detecting minor volatile constituents toward low-mass young stars from the ground, a study which is vitally important to understanding how our own system evolved.

The data presented herein were obtained at the W. M. Keck Observatory, which is operated as a scientific partnership among the California Institute of Technology, the University of California, and the National Aeronautics and Space Administration. The Observatory was made possible by the generous financial support of the W. M. Keck Foundation. T. W. R. was supported by NSF Astronomy grant AST 02-05581 and AST 05-07419. S. B. was supported in part by a NASA Michelson Fellowship (2005–2006). E. L. G. was supported by NSF Astronomy grant AST 05-07419.

## REFERENCES

- Aikawa, Y., Umembayashi, T., Nakano, T., & Miyama, S. M. 1999, *ApJ*, 519, 705  
 Aikawa, Y., van Zadelhoff, G. J., van Dishoeck, E. F., & Herbst, E. 2002, *A&A*, 386, 622  
 Boogert, A. C. A., Helmich, F. P., van Dishoeck, E. F., Schutte, W. A., Tielens, A. G. G. M., & Whittet, D. C. B. 1998, *A&A*, 336, 352  
 Boogert, A. C. A., Hogerheijde, M. R., & Blake, G. A. 2002, *ApJ*, 568, 761  
 Boogert, A. C. A., Schutte, W. A., Helmich, F. P., Tielens, A. G. G. M., & Wooden, D. H. 1997, *A&A*, 317, 929  
 Brittain, S. D., Rettig, T. W., Simon, T., & Kulesa, C. 2005, *ApJ*, 626, 283  
 Brittain, S. D., Rettig, T. W., Simon, T., Kulesa, C., DiSanti, M. A., & Dello Russo, N. 2003, *ApJ*, 588, 535  
 Devine, D., Reipurth, B., Bally, J., & Balonek, T. J. 1999, *AJ*, 117, 2931  
 DiSanti, M. A., Mumma, M. J., Dello Russo, N., & Magee-Sauer, K. 2001, *Icarus*, 153, 361  
 Gibb, E. L., Brittain, S. D., Rettig, T. W., Kulesa, C., & Simon, T. 2004, *ApJ*, 610, L113

- Gibb, E. L., Mumma, M. J., Dello Russo, N., DiSanti, M. A., & Magee-Sauer, K. 2003, *Icarus*, 165, 391
- Glassgold, A. E., Najita, J., & Igea, J. 2004, *ApJ*, 615, 972
- Goodrich, R. W. 1986, *AJ*, 92, 885
- Harris, G. J., Polyansky, O. L., & Tennyson, J. 2002, *ApJ*, 578, 657
- Hinkle, K., Wallace, L., & Livingston, W. 1995, *PASP*, 107, 1042
- Jacquemart, D., et al. 2003, *J. Quant. Spectrosc. Radiat. Transfer*, 82, 363
- Koresko, C. D., Blake, G. A., Brown, M. E., Sargent, A. I., & Koerner, D. W. 1999, *ApJ*, 525, L49
- Kunde, V. G., & Maguire, W. C. 1974, *J. Quant. Spectrosc. Radiat. Transfer*, 14, 803
- Lahuis, F., & van Dishoeck, E. F. 2000, *A&A*, 355, 699
- Lahuis, F., et al. 2006, *ApJ*, 636, L145
- Langer, W. D., & Penzias, A. A. 1990, *ApJ*, 357, 477
- Leinert, Ch., Beck, T. L., Ligorì, S., Simon, M., Woitas, J., & Howell, R. R. 2001, *A&A*, 369, 215
- Leinert, Ch., & Haas, M. 1989, *ApJ*, 342, L39
- Lyons, J. R., & Young, E. D. 2005, *Nature*, 435, 317
- Markwick, A. J., Ilgner, M., Millar, T. J., & Henning, Th. 2002, *A&A*, 385, 632
- McLean, I. S., et al. 1998, *Proc. SPIE*, 3354, 566
- Ménard, F., Monin, J.-L., Angelucci, F., & Rouan, D. 1993, *ApJ*, 414, L117
- Mumma, M. J., DiSanti, M. A., Dello Russo, N., Magee-Sauer, K., Gibb, E., & Novak, R. 2003, *Adv. Space Res.*, 31, 2563
- Rettig, T. W., Brittain, S. D., Simon, T., Gibb, E. L., Balsara, D. S., Tilley, D. A., & Kulesa, C. 2006, *ApJ*, 646, 342
- Rothman, L. S., et al. 2003, *J. Quant. Spectrosc. Radiat. Transfer*, 82, 5
- Vander Auwera, J., Hurtmans, D., Carleer, M., & Herman, M. 1993, *J. Mol. Spectrosc.*, 157, 337
- White, R. J., & Hillenbrand, L. A. 2004, *ApJ*, 616, 998
- Willacy, K., Klahr, H. H., Millar, R. J., & Henning, Th. 1998, *A&A*, 338, 995
- Wilson, T. L., & Rood, R. 1994, *ARA&A*, 32, 191